A computational hydrodynamics method for horizontal axis turbine - panel method modeling migration from propulsion to turbine energy

Liu, Pengfei

Publisher's version / Version de l'éditeur:
https://doi.org/10.1016/j.energy.2010.03.013
Energy, 35, 7, pp. 2843-2851, 2010-04-22

A Computational Hydrodynamics Method for Horizontal Axis Turbine --- Panel Method Modeling Migration from Propeller to Turbine

Pengfei Liu*
Institute for Ocean Technology, National Research Council Canada, 1 Kerwin Place and Arctic Avenue, Box 12093, St. John's, Newfoundland and Labrador, A1B 3T5 Canada

Abstract

A computational hydrodynamics method was formulated and implemented for horizontal axis tidal turbines. This paper presents a comparative analysis between screw propellers and horizontal axis turbines, in terms of geometry and motion parameters, inflow velocity analysis and the implementation methodologies. Comparison and analysis are given for a marine propeller model and a horizontal axis turbine model that have experimental measurements available in literature. Analysis and comparison are presented in terms of thrust coefficients, shaft torque/power coefficients, blade surface pressure distributions, and downstream velocity profiles. The effect of number of blades from 2 to 5, of a tidal turbine on hydrodynamic efficiency is also obtained and presented. The key implementation techniques and methodologies are provided in detail for the propeller based panel method tool to migrate as a prediction tool for tidal turbine. While the method has been proven to be accurate and robust for many propellers tested in the past, this numerical tool could be validated further for turbines. To further refine and validate the panel method for various turbines, it requires substantial additional experimental measurements. These measurements include downstream velocity profile by using LDV and/or SPIV, which are essential for numerical wake vortices descritization.

Keywords: panel method; propeller; wind turbine, tidal turbine hydrodynamics;

Nomenclature

α --- angle of attack of blade section
α' --- angle of attack of blade section with added induced velocity
α_p --- geometric angle of attack of blade section
α_o --- angle of zero lift of blade section
α_v --- angle of inflow velocity (hydrodynamic angle of attack)
$\alpha_{v'}$ --- angle of inflow velocity with added induced velocity
α_e --- effective angle of attack of blade section
C_t --- thrust coefficient of turbine
C_{POW} --- turbine power coefficient
C_P --- pressure coefficient
D --- diameter of turbine or propeller
EAR --- expanded area ratio of blades of propeller disk, or solidity of turbine.
h_D --- hub diameter to blade diameter ratio
J --- shaft advance coefficient
K_t --- shaft thrust coefficient
K_q --- shaft torque coefficient

* Corresponding author: Tel: (709) 772-4575, Fax: (709) 772-2462
E-mail address: pengfei.liu@nrc-cnrc.gc.ca

K_{sp} --- blade spindle torque
K_{ip} --- blade in-plane bending moment
K_{op}--- blade out-of-plane bending moment
n --- shaft rotational speed (rps)
p --- absolute pitch value at local radius r
p_D --- normalized pitch (p/D) at local radius r
r --- blade section local radius
R --- blade radius
TSR --- blade tip speed ratio
v_a --- advance speed of propeller shaft or inflow velocity of turbine
$v_{a'}$ --- advance speed or inflow velocity with added induced velocity
v_t --- induced tangential velocity at blade section
v_r --- induced radial velocity at blade section

1. Introduction

Computational methods have been widely used for wind or tidal turbine research and development. A comprehensive review of these methods and their merits and limitations, for example, was given by Nicholls-Lee et al. [1]. Among these methods, the panel methods, in the most advanced and complicated method group, have both high computing efficiency and prediction accuracy as an engineering tool for turbine simulation and design optimization. While probably the blade element methods (BEM) are the most widely used as preliminary simulation tools for wind and tidal turbines, much fewer penal methods could be found for turbine in literature. To the author's knowledge, these few panel methods for turbine simulation and prediction include a 2D panel method by Drela et al. mentioned in [1], a 3D time domain panel method for wind turbine by Hampsey [2], a rudder-propeller interaction panel code by Turnock [3] and a design based simulation work by Greco et al. [4]. Formulation and implementation of these panel methods for both wind turbines and tidal turbines are basically the same though different fluid properties such as viscosity/density and hence Reynolds number, require different scheme and numerical treatment. The primary difference for panel methods as tools for wind turbine and for tidal turbine is that tidal turbines are often exposed to cavitation that would cut off the negative pressure spike and reduces the energy extraction efficiency substantially even if there does not exist stall or separation. For wind turbine under high speed inflow conditions, compressibility might need to be a problem, at least in terms of turbine efficiency correction. A bare panel method developed from scratch also needs many other essential numerical components for different application cases. Establishing these numerical components for a newly developed bare panel method require substantial effort and implementation development, as described later in this section. In this paper, it shows an efficient turn-key solution that a well established propeller panel method can be quickly turned into a turbine simulation code.

Panel methods, are called the boundary element methods, or boundary integral methods (BEM in short as well). Lifting surface and panel methods have been widely used in research and development of aircraft wings, hydrofoils and both aerial and marine propellers. Zero thickness propeller blade simulated and computed by lifting surface theory in the computational fluid dynamics (CFD) field has a history of over 60 years. The use of the surface panel method for a simple body surface mesh can be traced back to the early 1960s. Hess and Vararezo [5] probably made the first panel method computation for propellers. To deal with complete aircraft geometry, panel method codes, PMARC (Panel Method Ames Research Center) developed by Katz [6] and VSAERO by Maskew [7] are the early examples of panel methods for aircraft wings and propellers. On the other hand, panel methods have also been used for marine propeller research development and early examples among those are publications by Kerwin [8] and Hoshino [9], just to name a few. A time domain unsteady panel method code OSFBEM (oscillating foil boundary element method) was developed by the author for oscillating propulsors of both chordwise and spanwise flexibility to simulate marine animals' propulsion [10]. To respond the need in simulation of fluid-structure interactive hydrodynamics to predict ice blockage effects between ice sheet and ice-class propellers, a panel method code, PROPELLA [11] was developed in 1996, based OSFBEM. Since then, continued efforts were made to maintain and enhance the capability for the code. The capability for unsteady oblique flow and inflow wake were presented in early 1998 [12]. Automatic body surface generation for propeller of arbitrary number of blades, nozzle, rudder, ice blockage etc. was presented in 2001, along with velocity profile downstream prediction and wake vortices roll-up enhancement [13]. Cavitation predictive capability via an empirical formulation was established for PROPELLA and presented in 2001 [14]. At the meantime, a pre- and postprocessor was developed for the code by using OpenGL and Visual C++ of Microsoft Foundation Class, as a 3D unsteady data visualization tool [15] to view the geometry motion and colour blended results. A novel and robust numerical Kutta condition using Broyden's iteration was developed and presented in 2002 [16]. Since 2003, this propeller panel method has been redeveloped with a multiple-body interaction formulation to deal with a propeller with pod and strut, called a podded propeller unit and recently for a podded propulsor interacting with an ice body at variable proximity (transient hydrodynamic response of a propeller moving towards an ice sheet) [17]. In the past decades, many panel methods have been developed and these panel methods along with their associated numerical schemes and techniques for propellers are well established. These existing panel methods with a minor or moderate revision, could be quickly used for tidal and wind turbine prediction. The aim of this work is to present the physics and numerical similarities and difference between propeller and turbine panel methods and then provide a detailed implementation techniques and treatments.

2. Method

The current panel method is a multiple-body interaction panel method. The fundamentals of panel method have been presented in detail in some textbooks, including the ones by Moran [18] for 2D foil sections and by Katz and Plotkin [19] for unsteady 3D body and wings. A detailed formulation and implementation for a low-order, time-domain panel method, were given by the author [10].

2.1. Flow Physics Similarity and Differences between Propeller and Tidal Turbine

Being rotary wings, flow around both propeller and turbine blade sections has both similarities and differences. Flow conditions around a wing section determine the hydrodynamic characteristics of the wing section. These characteristics are mainly determined by the effective angle of attack of the blade section. The similarity and differences of the flow around a blade section between propeller and turbine are shown in the velocity diagrams in Figures 1 and 2, respectively.

In Fig. 1, blade geometric pitch angle of attack is represented as α_P, and the angle of zero life of the blade section is α_0 due to the camber of the blade section. Therefore the effective geometric angle of pitch is $\alpha_P + \alpha_0$. The inflow velocity angle of attack, also called hydrodynamic angle of attack in the literature, is $\alpha_V = \tan^{-1}(\frac{V_a}{2\pi rn})$, where V_a is propeller shaft forward velocity, also called inflow velocity in some literature, and r is the blade section local radius and n is the shaft rotation speed in revolutions per second. However, even in open water, as a propeller is rotating, the inflow velocity to the propeller plane is not unidirectional because of the induced tangential velocity V_t and radial velocity V_r. In fact, these induced velocities are not in the same plane as shown in the figure. The total inflow velocity relative to the local blade section in 3D space is then $\vec{V}_a + \vec{V}_t + \vec{V}_r$ with the resultant velocity angle of attack α_V'. Therefore, the effective angle of attack of the blade section, that determines the hydrodynamic characteristic of a blade section, is $\alpha_e = \alpha_P + \alpha_0 - \alpha_V'$ for which induced velocities have been taken into account and is $\alpha = \alpha_P - \alpha_V$ without including the induced velocities and angle of zero life. It is obvious that for a propeller to produce positive thrust, i.e., to be in propulsion mode, the effective angle of attack must be positive. In the current version of the code PROPELLA, the angle of shed wake vortices at the blade trailing edge is taken as α at $r = 0.7000R$, where R is the radius of the propeller, when the angle of zero life is

neglected. When shed wake vortices roll-up is taken into account, the angle of shed wake vortices is modified by the induced velocity during a wake vortex relaxation procedure. While the pitch angle of shed wake vortices has substantial effect on the prediction accuracy of thrust and torque prediction, it is even more important to the accuracy of the field velocity prediction downstream of a propeller. In addition, to avail a multiple-body computational capability, all bodies in the fluid domain move individually in an acquiescent fluid.

A similar blade section velocity diagram for turbine is shown in Fig. 2. With all the same variables as those for propeller, the offset coordinates of the surfaces of propeller blade section are now interchanged, i.e., the suction side and pressure side of the blade section are swapped for a turbine. The effective angle of attack now becomes $\alpha_e = \alpha_V^{'} - \alpha_P + \alpha_0$ when the induced velocities are taken into account and $\alpha = \alpha_V - \alpha_P$ when the induced velocities and angle of zero lift are both neglected. It is also obvious that the effective angle of attack must be positive for the blade section to be in turbine mode. Now using the propeller code PROPELLA for turbine prediction is reduced to two key modifications when preparing for input, that is, the blade sectional coordinates interchange and the formulation and implementation of the angle of shed wake vortices. Using the same motion and geometric variables for propellers, the angle of shed wake vortices for a turbine is taken as α at local radius of *0.7R*. In the following non-dimensional analysis, the wake pitch angle of turbine was obtained as follows:

$$\alpha = \tan^{-1}\frac{V_a}{2\pi r n} - \tan^{-1}\frac{np}{2\pi r n} = \tan^{-1}\frac{JnD}{2\pi r n} - \tan^{-1}\frac{\frac{p}{D}D}{2\pi r} = \tan^{-1}\frac{J}{\pi\frac{r}{R}} - \tan^{-1}\frac{p_D}{\pi\frac{r}{R}}, \quad (1)$$

where *J* is the advance coefficient, $J = \frac{V_a}{nD}$, of turbine and P_D is the local non-dimensional pitch, $p_D = \frac{p}{D}$, based on the diameter of turbine. The same as propeller simulation, turbine is moving in an acquiescent fluid; the pitch angle is taken for wake vortices formulation as $p_{WD} = J - p_D\,|_{0.7R}$. The angle of shed wake vortices for a propeller by using the similar formulation gives good thrust and torque prediction and induced velocity estimation downstream. However, for turbine mode after extensive numerical test runs, the angle of shed wake vortices with an additional angle of inflow taken as $p_{WD} = 2J - p_D\,|_{0.7R}$ gave better results. Hoshino [9] recommended a wake vortex descritization formulation based on LDV measurements downstream of a propeller, including wake pitch, wake contraction, ultimate wake region, and transition. This formulation is valid only for propulsion mode, not turbine mode. For turbine, if this wake vortex descritization is used, wake contraction becomes a substantial inflation (*800* times). This occurred at a low tip speed ratio

of about *TSR = 4.0000* corresponding to *J = 0.7855,* with a ratio of *J/[p/D]* at about *3*, in the tidal turbine example (see the results and discussion section below).

Fig. 3 shows the descritzied wake vortices behind a 3-blade P4119 propeller [21] at J=0.8330 and a 20ºroot pitch tidal turbine at *TSR = 7.0000 (J=0.4488)*. In this paper, the tidal turbine refers to the tidal turbine model by Bahaj et al. {22]. For presentation purposes, wake vortices in Fig. 3 are shown only for one blade.

2.2.Parametric Interpolation between Propeller and Tidal Turbine

The geometric parameters between a propeller blade and a tidal turbine are the same. For example, the expanded area ratio EAR is the ratio of the total blade area to the area of the propeller disk. Therefore the solidity of a turbine rotor is equivalent to the EAR of a propeller. For a tidal turbine calculation using a propeller code such as PROEPLLA, the only geometry manipulation needed to prepare for code input, is to interchange the blade upper side with the lower side, i.e. to swap the suction side and the pressure side. However, to extrapolate the results in propeller format corresponding to a turbine convention, three major variables need to be interpolated. They are advance coefficient *J* versus tip speed ratio *TSR*, propeller thrust coefficient K_t versus turbine thrust coefficient C_t, and propeller torque coefficient K_q versus power coefficient C_{pow}. With the definitions of propeller advance coefficient, $J = \frac{V_a}{nD}$, propeller thrust coefficient $K_t = \frac{T_{thrust}}{\rho n^2 D^4}$, propeller shaft torque coefficient $K_q = \frac{Q_{torque}}{\rho n^2 D^5}$, turbine tip speed ratio, $TSR = \frac{\omega R}{V_a}$, turbine thrust coefficient, $C_t = \frac{T_{thrust}}{\frac{1}{2}\rho V_a^2 A}$, and turbine power coefficient $C_{pow} = \frac{Q_{torque}\omega R}{\frac{1}{2}\rho V_a^3 A}$, the three parameters for tidal turbine in terms of propeller, are then

$$TSR = \frac{\omega R}{V_a} = \frac{2\pi n R}{V_a} = \frac{\pi n D}{V_a} = \frac{\pi}{J}, \tag{2}$$

$$C_t = \frac{T_{thrust}}{\frac{1}{2}\rho V_a^2 A} = \frac{K_t \rho n^2 D^4}{\frac{1}{2}\rho V_a^2 \pi R^2} = \frac{8K_t}{\pi J^2}, \quad \text{and} \tag{3}$$

$$C_{pow} = \frac{Q_{torque}\omega R}{\frac{1}{2}\rho V_a^3 A} = \frac{K_q \rho n^2 D^5 2\pi n R}{\frac{1}{2}\rho V_a^3 \pi R^2} = \frac{16K_q n^3 D^3}{V_a^3} = \frac{16K_q}{J^3}. \tag{4}$$

Therefore, for a desired *TSR* a value of corresponding advance coefficient *J* can be obtained for a propeller code. When the results K_t and K_q are obtained from a propeller code, they can be interpolated as C_t and C_{pow}, respectively, for turbine as a function of non-dimensional speed *J*.

3. Results and discussion

3.1. Geometry and Motion Parameters

Predictions for turbine hydrodynamic characteristics were obtained for a tidal turbine base model plus two root pitch offsets. For these models, experimental measurements are available for comparison. Table 1 shows, as an example, a list of coordinates for a foil section with 18.0000% thickness and a section profile shape of the NACA 63-8xx [23]. The turbine blade's sectional maximum thickness varies from 24.0000% at the root section to 15.6000% at the tip section.
A model propeller P4119 by David Taylor Model Basin (DTMB) along with its results is used for comparison [21, 24]. A surface panel mesh arrangement for the propeller and the tidal turbine model [12] are shown in figures 4.

To obtain a range of tip speed ratio *TSR* from *4.0000* to *10.0000*, corresponding input values of *J* and required shaft revolution speed *N* in rpm for a *0.8000-m* diameter tidal turbine model were obtained. These *J* values were calculated based on a constant inflow speed of *1.5000 m/s* to simulate the actual cavitation tunnel test conditions by Bahaj et al. [22] and are listed in Table 2.

Table 3 shows the sectional effective angle of attack (*AOA*) at shaft speed of *n =4.0000* rps corresponding to a *TSR* of *6.7021*. The values of the effective angle of attack are estimated when the induced velocity and angle of zero lift are neglected. In the work by Bahaj et al. [22], a base turbine model has a root pitch angle of *15°* with an offset degree of *5°* and *10°* to add another two more turbine models.

Examining the sectional effective *AOA* for the *15°, 20°* and *25°* root pitch angle turbines, it can be seen that the *15°* root pitch turbine is the most heavily loaded. The effective *AOA* at the tip section is about *8.5000°*, which will most likely result in a bad cavitation (cavitation analysis is a different topic so it is omitted here though PROPELLA has the capability to do so). The best sectional effective *AOA* among these three turbines is the 20° root pitch one, though a slight increase of effective AOA up to *5°* at the tip might give a better hydrodynamics efficiency. The *25°* root pitch turbine would give the

poorest hydrodynamic efficiency because the blade sections from *r/R = 0.8000* to the tip are all in propulsion mode (the effective AoA is negative by turbine AoA definition).

3.2. Turbine C_t and C_{pow} versus Propeller K_t and K_q

Figures 5, 6 and 7 show the thrust and power coefficient of the horizontal axis turbine with a root pitch angle of *15°, 20°* and *25°*.

As mentioned earlier in this section, the effective angles of attack of the blade section of the 15º root pitch turbine are abnormally large. These large values could most likely cause flow separation and stall. The separation and stall simulation is not implemented in the current method. It is noted too that the maximum power coefficient of the 15º root pitch turbine is just as high as about *0.4000* and this value diminishes at a TSR of about *6.0000*. This small production of power coefficient are most likely attributed separation and stall where potential flow based methods like the panel methods could not simulate (the higher the TSR, the worse the stall and separation and hence the larger the discrepancy between the method and measurements) . This indicates that the 15º root pitch angle turbine is operational only in a narrow range of tip speed ratio with pretty poor hydrodynamic efficiency.

In Fig. 7, a better hydrodynamic performance is shown for the 20º root pitch angle turbine. The current method produced a slightly lower thrust coefficient and higher power coefficient, compared with the measurements, than that of the 15ºroot pitch turbine, especially operating under at large tip speed ratio close to 10.0000. It noted that the maximum power coefficient occurred at the tip speed ratio *TSR* of 6.0000 for measurements but occurred at about a *TSR* of 7.5000 for the prediction.

A general agreement between the measurements and the prediction by the current method can also be seen for the 25ºroot pitch angle turbine. As mentioned earlier in this section, blade tip sections at more than 80%R radial locations have negative effective angle of attack and hence they do negative work. This caused a much small power coefficient compared with the 20ºone (0. 3900 versus 0.4500).

As mentioned earlier for wake vortices descritization, the wake pitch angle has a strong influence on the prediction accuracy of the method. Taking a proper value of wake pitch will ensure not only the accuracy of predicted thrust and

power coefficients but also for the velocity profile downstream. At the moment, lack of sufficient tidal turbine measurements on thrust and power coefficients, and experimental data by LDV or PIV for the velocity profile downstream of a tidal turbine, makes it difficult for numerical method validation. Fig. 8 shows a set of thrust and power coefficient for the DTMB propeller by the current method PROPELLA.

It can be seen that prediction by PROPELLA agreed very well with the measurements. As described above, the wake pitch was taken as the value of the angle of attack at *0.7000R* and this wake pitch seems a proper one based on the close agreement between the prediction and the measurements. Further comparison will be given for the induced velocity at a location downstream of propeller and turbine.

3.3. Pressure Distribution of a Propeller versus the a Tidal Turbine

Fig. 9 shows the pressure distribution on the blade surface of the DTMB P4119 propeller at an advance coefficient of *J=0.8330*. It can be seen that the values of the pressure coefficient on the back side of the blade (viewing from downstream) are mainly negative and vise versa. Therefore the back side of a propeller blade is often referred to suction side and the face side is referred to the pressure side, when operating in the propulsion mode at the first quadrant (positive rotational speed and positive forward speed). After a robust numerical Kutta condition was applied, the pressure difference between the suction side and the pressure side at the trailing edge, as can be see in the figure, is close to zero.

Fig. 10 shows color blended pressured distribution on the suction side of the DTMB P4119 propeller blade (viewing from upstream). Both the propeller and turbine were modelled as right-handed revolution propeller/rotor viewing from downstream.

Fig. 11 shows the pressure distribution on a blade of the 20ºroot pitch tidal turbine at *TSR = 7.0000*. It is noted that, contrary to propeller, the values of the pressure coefficients on the back side of the tidal turbine (viewing from downstream) are mainly positive and these on face side are mainly negative. The back side now becomes pressure side and vice versa.. It also can be seen that the values of the suction side pressure of the tidal turbine could possibly cause sever cavitation that would deteriorate the hydrodynamic performance substantially, if the shaft immersion depth of tidal turbine is sufficiently small.

Fig. 12 shows the color blended pressure coefficient distribution on the surface of the right-handed rotation tidal turbine blades, viewing from downstream. It can be seen that high pressure occurs at the trailing edge of the blade sections and the pressure coefficient decreases with the chord location towards the leading edge.

3.4.Downstream Velocity Profile: Propeller versus Tidal Turbine

A comparison on velocity profile downstream of the propeller and the tidal turbine is discussed below. Fig. 13 shows the velocity profile in a plane at 0.16405 diameter behind the propeller predicted by the current panel method PROPELLA compared with the measurement by using LDV [21]. It is noted that the tangential velocity is in the same direction with the revolution direction of the propeller shaft. The axial velocity at the plane pointing downstream but radial velocity is negative, parallel to centre-line of the shaft. The negative radial velocity means that the shed wake vortices at this plane are in contraction.

Fig. 14 presents the predicted velocity profile at a plane of 0.16405 diameter downstream of the tidal turbine at $TSR = 7.0000$. Contrary to propeller, the radial velocity at the plane is positive which means that the wake vortices tend to inflate. The tangential velocity is opposite to the rotation of the turbine with negative sign except the tip. The axial velocity is negative as well indicating that the flow past the blades of the turbine has a decrease in velocity.

The opposing direction of the downstream velocities of a propeller against that of a turbine also indicates that propeller in operation transfer energy to the fluid to accelerate the inflow, while turbine extracts energy by absorbing the momentum of the fluid and ends up a slowing down the inflow.

3.5. Number of Blade Effect on Hydrodynamic Efficiency of Tidal Turbines

A numerical investigation was also made to examine the effect of number of blades on the hydrodynamic efficiency (power coefficient) for a turbine of 2, 3, 4 and 5 blades with the same solidity, i.e., expanded area ratio $EAR=0.0669$. Fig. 15 shows the surface solid modeling of the turbine geometry for the 4 turbines of different number of blades.

Fig. 16 presents a comparison of the hydrodynamic efficiency (power coefficients) among the 2-, 3-, 4- and 5-blade tidal turbines. The geometry of the 4 tidal turbines was generated by a constant expanded area ratio the same as the 3-blade tidal

turbine model. The chord length of the turbine blades was enlarged proportionally for the 2-blade turbine and reduced for the 4- and 5-blade turbines. It shows in Fig.18, with the increase of the number of blades, that power coefficients dropped gradually and proportionally. With the increase of the number of blades, the *TSR* values at which the maximum power coefficients *TSR* occur, shift to the left (reduced), from *TSR= 8.0000* for the 2-blade tidal turbine to *TSR = 6.5000* for the 5-blade one.

4. Conclusion

A time-domain, low order panel method was developed for tidal turbine performance evaluation, design and optimization, based on a well established and robust propeller code PROPELLA. Familiarities and differences in hydrodynamic characteristic between propeller and turbine were discussed in terms of blade section flow velocity diagram and effective angle of attack. Detailed methodology and techniques were presented for propeller panel method applied to migrate to simulation for turbines. Predictions for a propeller and a turbine model were obtained and compared. These predictions showed a general agreement with the measurements. Blade surface pressure distributions and the downstream velocity profile of the tidal turbine model obtained are contrary to a propeller. A numerical investigation was performed for 4 turbines with the same geometry shape and same expanded area ratio with a different number of blades ranging from 2 to 5. Results indicate that with the increase of the number of blades, the power coefficients decrease dramatically and proportionally. It was also noted that the optimum *TSR* at which the highest power coefficient occurs shifts left (reduces) with the increase of the number of blades, from *TSR =8.0000 to 6.5000*. While the propeller panel method was developed with a huge amount of measurement data to validate it, there is a need for substantial experimental data on wake vortices and downstream velocity profile by LDV and/or SPIV.

Acknowledgement

The author thanks to National Research Council Canada for its support. He is also grateful to Mr. Derek Yetman and Dr. Bruce Parsons for their proofread of the manuscript.

References

[1] Nicholls-Lee, Rachel F. , Turnock, Stephen R. and Boyd, Stephen W. Simulation Based Optimization of Marine Current Turbine Blades, In, Betram, Volker and Rigo, Philippe (eds), 7th International Conference on Computer and IT Applications in the Marine Industries (COMPIT'08), Liege; 21-23 April 2008, pp 314-328.

[2] Hampsey, Mark. Multiobjective Evolutionary Optimization of Small Wind Turbine Blades. PhD thesis, University of Newcastle, Australia; August 2002, 468 p.

[3] DTI. Economic viability of a simple tidal stream energy device, UK Department of Trade and Industry, Contract No.TP/3/ERG/6/1/15527/REP; 2007

[4] Greco, Luca, Testa, Claudio, and Salvatore, Francesco. Design Oriented Aerodynamic Modeling of Wind Turbine Performance. Journal of Physic: Conference Series 75(2007) 012011; 2007; DOI:10.1088/1742-6596/75/1/012011.

[5] Hess J.L., Vararezo W.O. Calculation of Steady Flow about Propellers by Mean of Surface Panel Method, Proceedings of Research and Technology, Douglas Aircraft Company, Long Beach, CA; 1985.

[6] Ashby D.L., Dudley M.R., Iguchi S.K., Browne L., Katz J. Potential Flow Theory and Operation Guide for the Panel Code PMARC, NASA TM 102851, 99 p.; 1991.

[7] Maskew B. Program VSAERO Theory Document, NASA Contractor Report 4023; 1986.

[8]. Greeley D.S., Kerwin J.E. Numerical methods for propellers design and analysis in steady flow, *Trans. SNAME* **90;** 1982, pp. 415–453.

[9] Hoshino T. Hydrodynamic Analysis of Propellers in Steady Flow Using a Surface Panel Method, 2nd Report, Flow Field around Propeller, Autumn Meeting of the Society of Naval Architects of Japan; Nov. 1989, pp. 79-92.

[10] Liu P. A time-domain Panel Method for Oscillating Propulsors with both Chordwise and Spanwise Flexibility, PhD Thesis, Memorial University of Newfoundland, Canada; 1996.

[11] Liu P. Software Development on Propeller Geometry Input Processing and Panel Method Predictions of Propulsive Performance of the R-Class Propeller, Progress Report on Transport Canada Ice-Class Propeller Research Project (TDC Contract #T8200-6-6507-001/XSD), MMC Engineering & Research, Newfoundland, Canada; 1996

[12] Liu P., Bose N. An Unsteady Panel Method for Highly Skewed Propellers in Non-Uniform Inflow, 22nd ITTC Propulsion Committee Propeller RANS/Panel Method Workshop, 5-6 April, Grenoble, France; 1998, pp. 343-349.

[13] Liu P., Bose N., Colbourne B. Automated Marine Propeller Geometry Generation of Arbitrary Configurations and a Wake Model For far Field Momentum Prediction, Int. Shipbuild. Progr., 48, no. 4 (2001) pp. 351-381.

[14] Liu P., Base N., Colbourne B. Incorporation of a critical pressure scheme into a time-domain panel method for propeller sheet cavitation, International Workshop on Ship Hydrodynamics, Wuhan, China; 2001 China, 9p.

[14] Liu. P. Design and Implementation for 3D unsteady CFD Data Visualization Using Object-Oriented MFC with OpenGL: Journal of Japan Society of Computational Fluid Dynamics, vol. 11, no. 3, October 2002; pp. 335-345.

[15] Liu P., Bose N., Colbourne B. A Broyden numerical Kutta condition for an unsteady panel method, Int. Shipbuild. Progr., 2002; 49, no. 4, pp. 263-273.

[16] Liu P., Akinturk A., He M., Islam M., Veitch B. Hydrodynamic performance evaluation of an ice class podded propeller under ice interaction, OMAE2008-57013, Proceedings of 27th International Conference on Offshore Mechanics and Arctic Engineering; 2008, 9 p.

[17] Moran J. Introduction to Theoretical and Computational Aerodynamics, John Wiley and Sons, New York; 1984.

[19] Katz J., Plotkin, A. Low-speed aerodynamics: from wing theory to panel methods, McGraw-Hill; 1991.

[20] Liu. *P.* Propulsive performance of a twin-rectangular-foil propulsor in a counter-phase oscillation*,* Journal of Ship Research, Vol. 49, No. 3, 2005; pp. 207-214.

[21] Jessup J. An Experimental Investigation of Viscous Aspects of Propeller Blade Flow, PhD Thesis, The Catholic University of America; 1989, 249p.

[22] Bahaj A.S., Batten W.M.J., McCann G. Power and Thrust measurement of marine current turbines under various hydrodynamic flow conditions in a cavitation tunnel and a towing tank, Renewable Energy 32 (2007) pp. 407-426.

[23] Abbot I.H., von Doenhoff A.E. Theory of Wing Sections, Dover Publications, Inc.; 1949, 693 p.

[24] Gindroz B., Hoshino T., Pylkkanen J.V. Proceedings of 22nd ITTC Propulsion Committee Propeller RANS/Panel Method Workshop, Grenoble, France; 1998.

List of Figures:

List of Tables:

Figures 1-16:

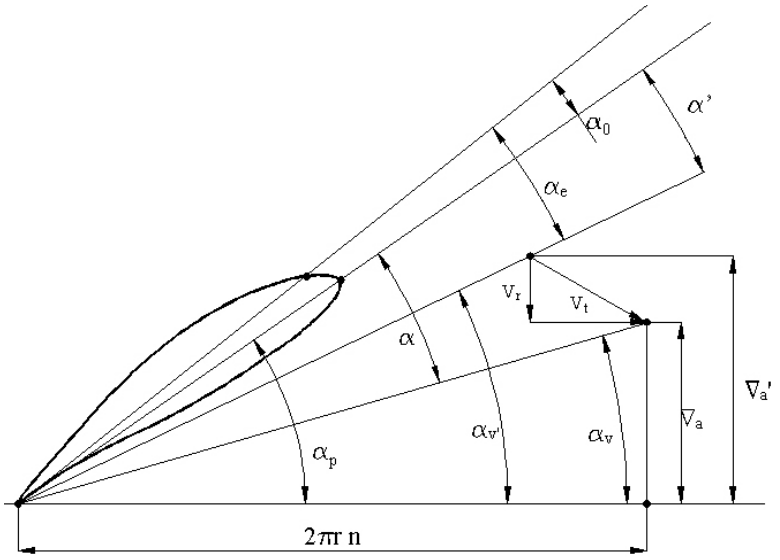

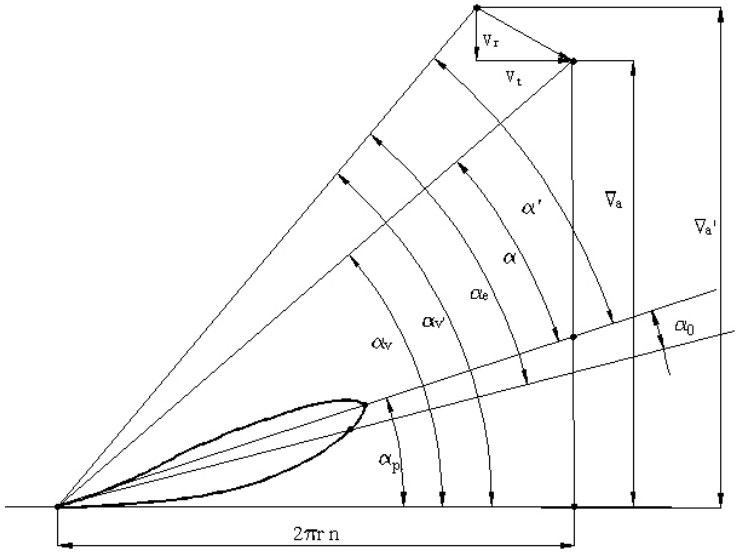

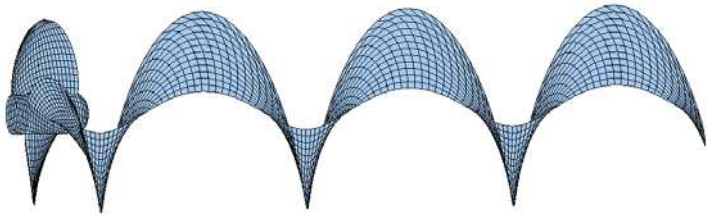

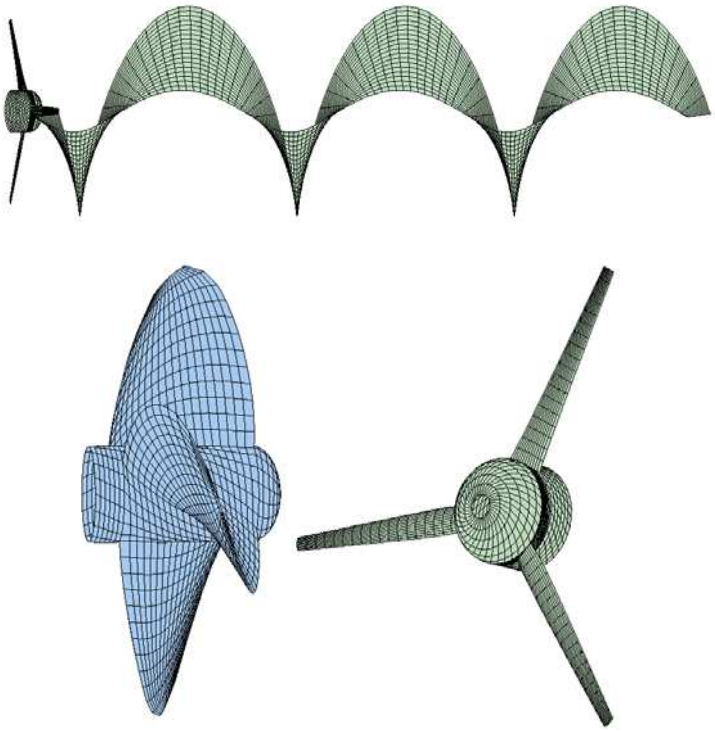

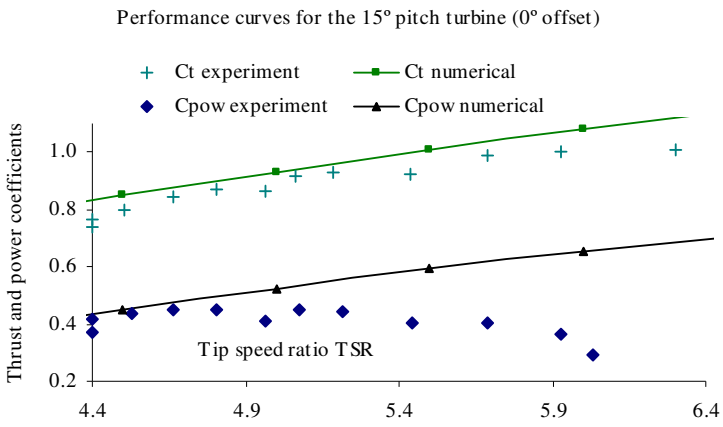
Performance curves for the 15° pitch turbine (0° offset)
Ct experiment
Ct numerical
Cpow experiment
Cpow numerical
Thrust and power coefficients
1.0
0.8
0.6
0.4
0.2
Tip speed ratio TSR
4.4
4.9
5.4
5.9
6.4

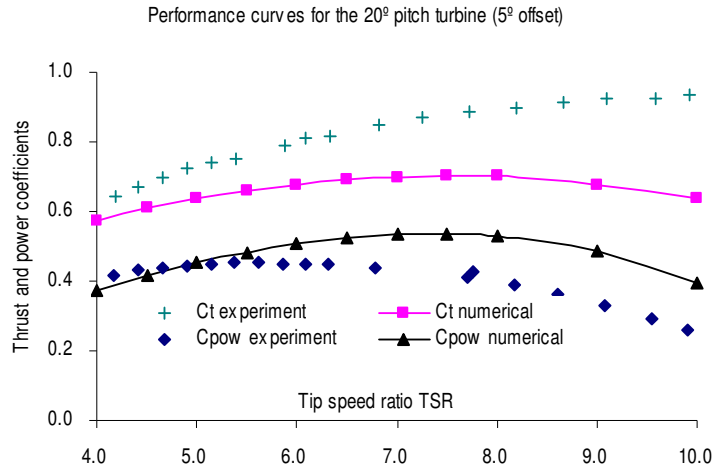
Performance curves for the 20º pitch turbine (5º offset)
Thrust and power coefficients
1.0
0.8
0.6
0.4
0.2
0.0
4.0
5.0
6.0
7.0
8.0
9.0
10.0
Ct experiment
Cpow experiment
Ct numerical
Cpow numerical
Tip speed ratio TSR

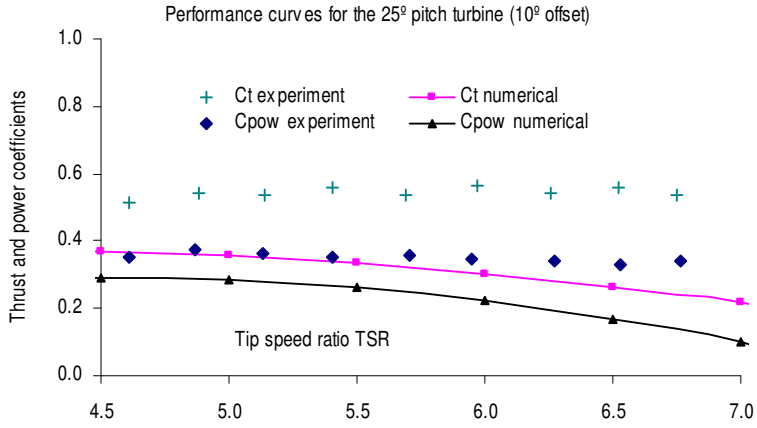
Performance curves for the 25º pitch turbine (10º offset)
Thrust and power coefficients
1.0
0.8
0.6
0.4
0.2
0.0
4.5
5.0
5.5
6.0
6.5
7.0
Ct experiment
Cpow experiment
Ct numerical
Cpow numerical
Tip speed ratio TSR

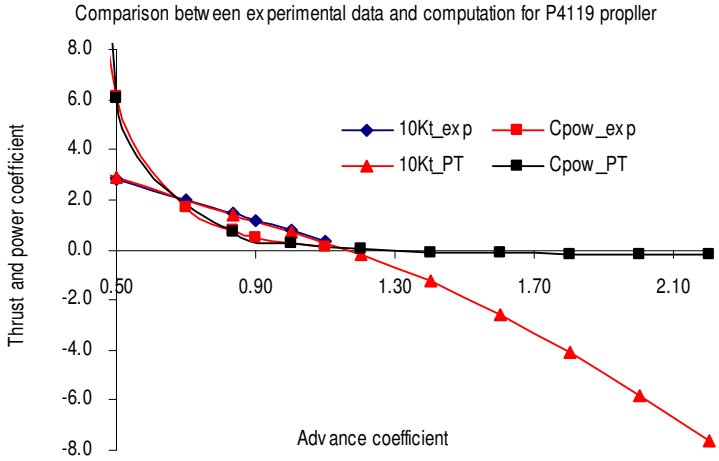
Comparison between experimental data and computation for P4119 propller
Thrust and power coefficient
8.0
6.0
4.0
2.0
0.0
-2.0
-4.0
-6.0
-8.0
0.50
0.90
1.30
1.70
2.10
10Kt_exp
Cpow_exp
10Kt_PT
Cpow_PT
Advance coefficient

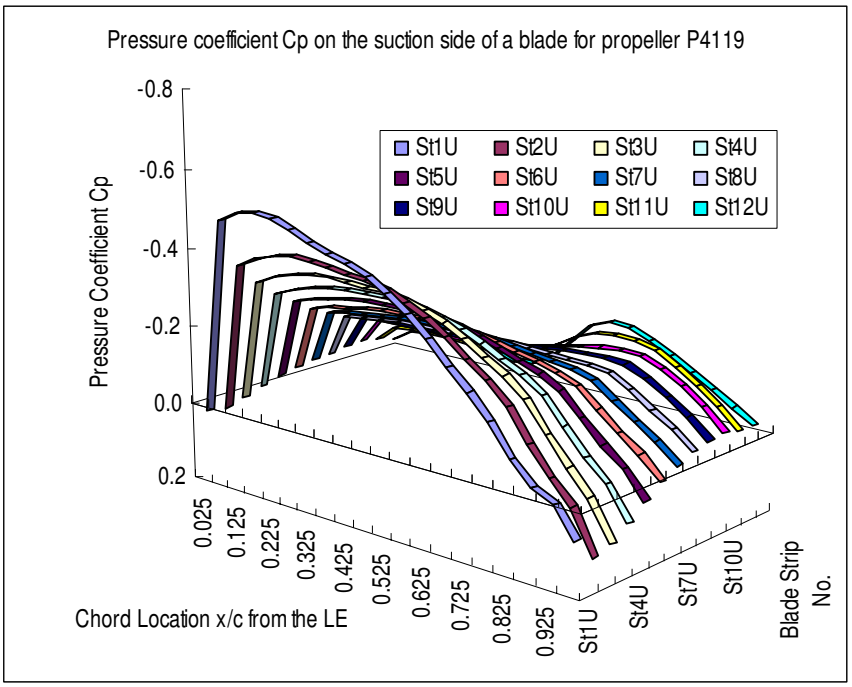
Pressure coefficient Cp on the suction side of a blade for propeller P4119
Pressure Coefficient Cp
-0.8
-0.6
-0.4
-0.2
0.0
0.2
St1U
St2U
St3U
St4U
St5U
St6U
St7U
St8U
St9U
St10U
St11U
St12U
0.025
0.125
0.225
0.325
0.425
0.525
0.625
0.725
0.825
0.925
Chord Location x/c from the LE
St1U
St4U
St7U
St10U
Blade Strip No.

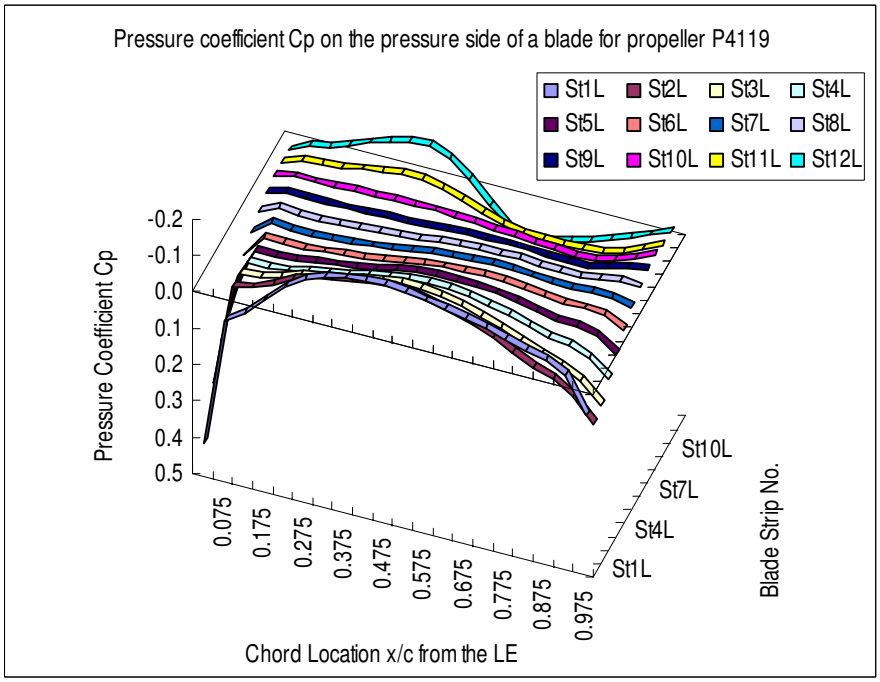
Pressure coefficient Cp on the pressure side of a blade for propeller P4119
Pressure Coefficient Cp
-0.2
-0.1
0.0
0.1
0.2
0.3
0.4
0.5
St1L
St2L
St3L
St4L
St5L
St6L
St7L
St8L
St9L
St10L
St11L
St12L
0.075
0.175
0.275
0.375
0.475
0.575
0.675
0.775
0.875
0.975
Chord Location x/c from the LE
St1L
St4L
St7L
St10L
Blade Strip No.

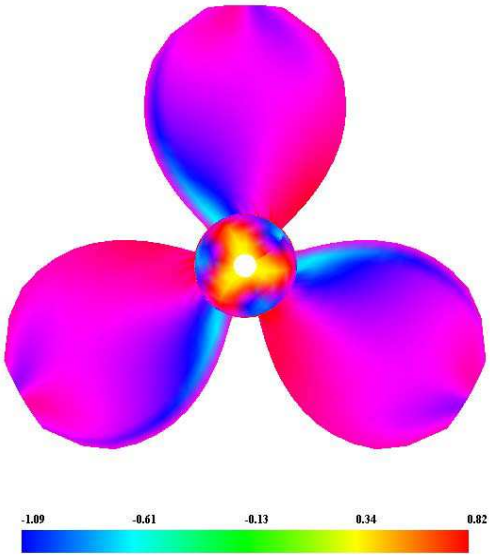
-1.09
-0.61
-0.13
0.34
0.82

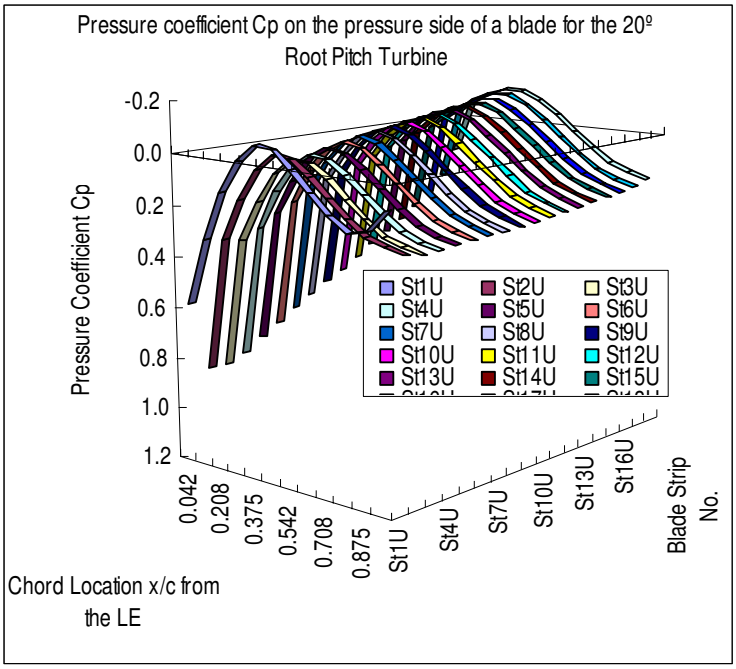
Pressure coefficient Cp on the pressure side of a blade for the 20º Root Pitch Turbine
Pressure Coefficient Cp
-0.2
0.0
0.2
0.4
0.6
0.8
1.0
1.2
St1U
St2U
St3U
St4U
St5U
St6U
St7U
St8U
St9U
St10U
St11U
St12U
St13U
St14U
St15U
0.042
0.208
0.375
0.542
0.708
0.875
St1U
St4U
St7U
St10U
St13U
St16U
Blade Strip No.
Chord Location x/c from the LE

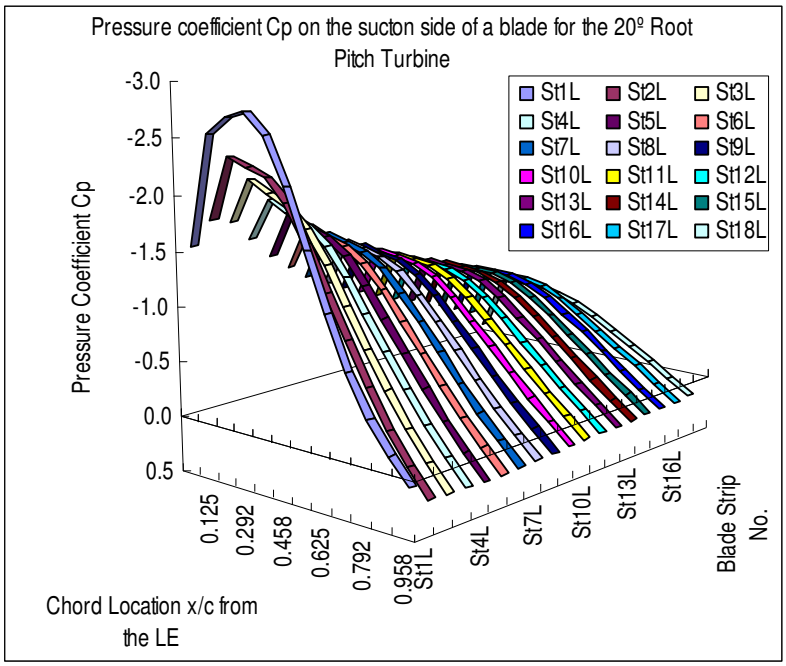
Pressure coefficient Cp on the sucton side of a blade for the 20º Root Pitch Turbine
Pressure Coefficient Cp
-3.0
-2.5
-2.0
-1.5
-1.0
-0.5
0.0
0.5
St1L St2L St3L
St4L St5L St6L
St7L St8L St9L
St10L St11L St12L
St13L St14L St15L
St16L St17L St18L
0.125
0.292
0.458
0.625
0.792
0.958
St1L
St4L
St7L
St10L
St13L
St16L
Blade Strip No.
Chord Location x/c from the LE

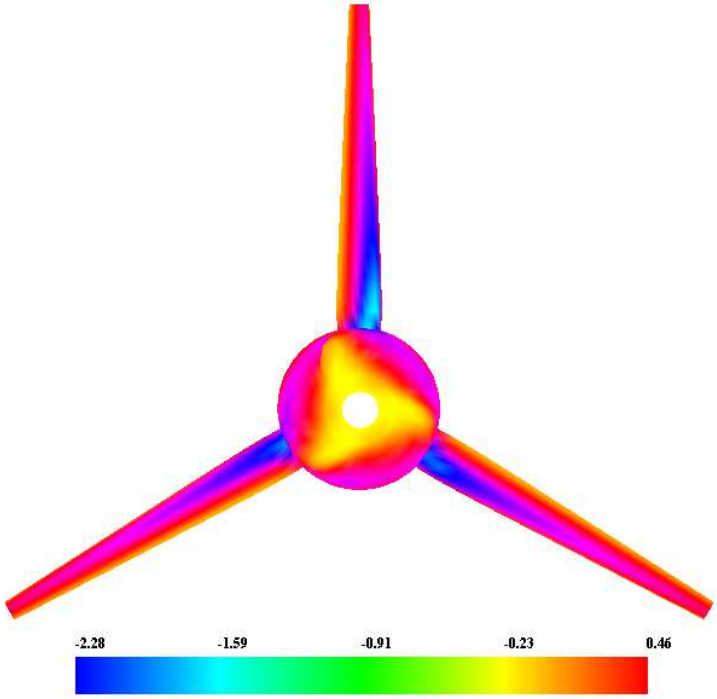
-2.28
-1.59
-0.91
-0.23
0.46

Circumferential averaged axial, tangential and radial velocities of P4119
at J=0.833 at x=0.16405D, PROPELLA versus 2-D LDV measurements

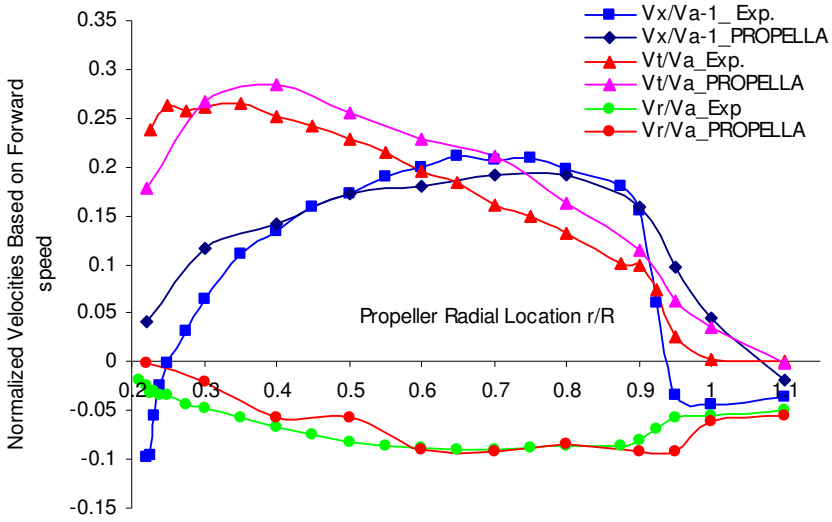

Circumferential averaged axial, tangential and radial velocities of the 20º
root pitch turbine model at TSR = 7.0 at x = 0.16405D (dow nstream)

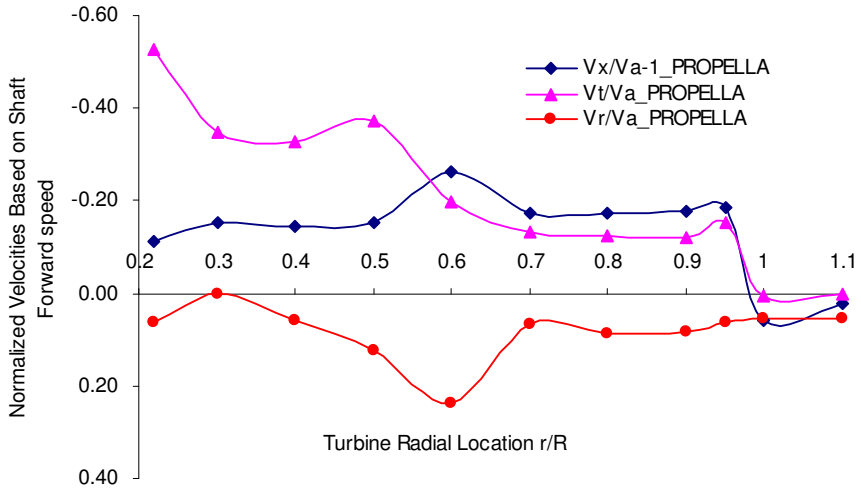

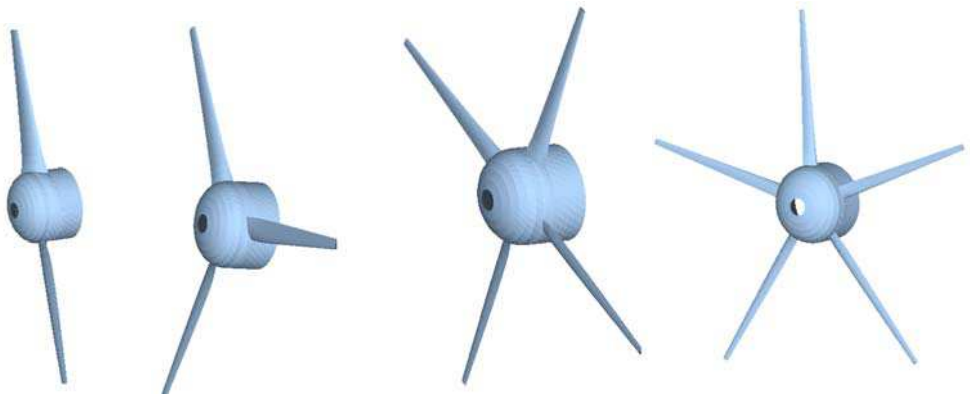

Power Coefficients C_{pow} of the 20° root pitch turbine with 2, 3, 4 and 5 blades at the same EAR 0f 0.0669

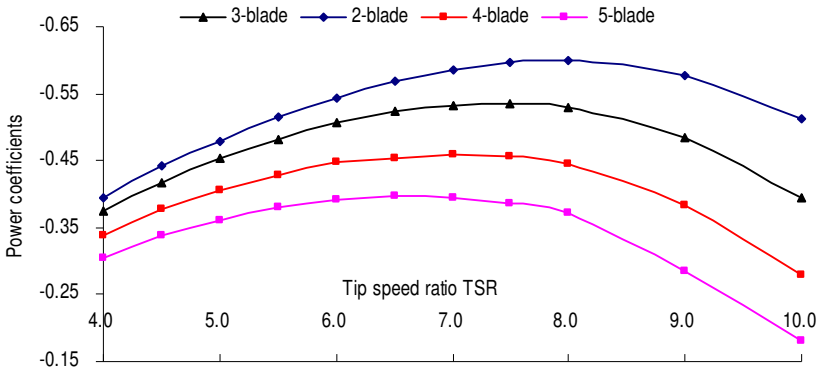

Tables 1-3:

X_{up}/c %	Y_{up}/c %	X_{low}/c %	Y_{low}/c %
0.0000	0.0000	0.0000	0.0000
0.1180	0.3830	0.0971	-0.4639
0.6380	0.7660	0.1943	-0.9278
1.4525	1.4020	0.3885	-1.9963
2.5572	1.9886	1.2782	-3.1285
4.0489	2.5317	2.5561	-4.3138
5.8763	3.0233	4.2510	-5.5421
8.0182	3.4889	6.3561	-6.7491
10.4830	3.8984	8.8287	-7.9177
13.2733	4.2623	11.6263	-9.0046
16.3429	4.5514	14.7503	-10.0473
19.6417	4.8009	18.2008	-10.9646
23.2062	4.9687	21.8870	-11.7551
26.9727	5.0470	25.8143	-12.4000
30.9059	5.0316	29.9560	-12.8741
34.9885	4.9166	34.2642	-13.1506
39.1988	4.6685	38.6933	-13.1997
43.5016	4.2981	43.2089	-13.0304
47.8647	3.8230	47.7721	-12.6568
52.2564	3.2669	52.3428	-12.1006
56.6441	2.6568	56.8814	-11.3890
60.9941	2.0207	61.3497	-10.5519
65.2710	1.3861	65.7122	-9.6201
69.4376	0.7816	69.9365	-8.6241
73.4647	0.2361	73.9842	-7.5891
77.3220	-0.2318	77.8207	-6.5546
80.9707	-0.6097	81.4227	-5.5540
84.3683	-0.8867	84.7744	-4.6091
87.4984	-1.0145	87.8379	-3.7278
90.3285	-1.0823	90.5957	-2.9261
92.8330	-0.9976	93.0286	-2.2125
94.9842	-0.9183	95.1243	-1.5961
96.7612	-0.5934	96.8698	-1.0256
98.1696	-0.3354	98.2310	-0.5796
99.1837	-0.1496	99.2111	-0.2585
99.7955	-0.0375	99.8024	-0.0647
100.0000	0.0000	100.0000	0.0000

TSR	*J*	*n = Va/J/D*	*N (rpm)*
4.0000	0.7854	2.3873	143.2394
4.5000	0.6981	2.6857	161.1444
5.0000	0.6283	2.9842	179.0493
5.5000	0.5712	3.2826	196.9542
6.0000	0.5236	3.5810	214.8592
6.5000	0.4833	3.8794	232.7641
7.0000	0.4488	4.1778	250.6690
7.5000	0.4189	4.4762	268.5740

8.0000	0.3927	4.7746	286.4789
9.0000	0.3491	5.3715	322.2888
10.0000	0.3142	5.9683	358.0986

r/R	ωr	$V_{resutant}$	$\tan^{-1}\frac{V_a}{\omega r}$	*α (15° pitch)*	*α (20° pitch)*	*α (25° pitch)*
0.2000	2.0106	2.5085	36.7244	21.7244	16.7244	11.7244
0.2500	2.5133	2.9269	30.8301	18.7301	13.7301	8.7301
0.3000	3.0159	3.3684	26.4439	16.9439	11.9439	6.9439
0.3500	3.5186	3.8250	23.0889	15.4889	10.4889	5.4889
0.4000	4.0212	4.2919	20.4565	14.3565	9.3565	4.3565
0.4500	4.5239	4.7661	18.3441	13.4441	8.4441	3.4441
0.5000	5.0265	5.2456	16.6159	12.7159	7.7159	2.7159
0.5500	5.5292	5.7291	15.1783	12.0783	7.0783	2.0783
0.6000	6.0319	6.2156	13.9650	11.5650	6.5650	1.5650
0.6500	6.5345	6.7045	12.9283	11.0283	6.0283	1.0283
0.7000	7.0372	7.1953	12.0327	10.5327	5.5327	0.5327
0.7500	7.5398	7.6876	11.2517	10.0517	5.0517	0.0517
0.8000	8.0425	8.1812	10.5648	9.6648	4.6648	-0.3352
0.8500	8.5451	8.6758	9.9562	9.3562	4.3562	-0.6438
0.9000	9.0478	9.1713	9.4132	9.0132	4.0132	-0.9868
0.9500	9.5504	9.6675	8.9260	8.7260	3.7260	-1.2740
1.0000	10.0531	10.1644	8.4864	8.4864	3.4864	-1.5136